Structural and electronic distortions in individual carbon nanotubes under laser irradiation in the electron microscope

David Rossouw, Matthieu Bugnet, and Gianluigi A. Botton*

Department of Materials Science and Engineering, Brockhouse Institute for Materials Research and Canadian Centre for Electron Microscopy, McMaster University, 1280 Main Street West, Hamilton, Ontario L8S 4M1, Canada

(Received 3 January 2013; revised manuscript received 6 February 2013; published 5 March 2013)

Correlated electronic and structural distortions in individual carbon nanotubes induced by photon excitation are observed for the first time by using a unique *in situ* transmission electron microscope configuration. By combining sub-100-meV resolution electron energy-loss spectroscopy with *in situ* photon excitation of the specimen, we are able to measure carbon nanotube expansions coupled to electronic transitions in their density of states as a direct consequence of the photon excitation/irradiation. Laser-induced effects are recorded in electron energy-loss spectra, which show reversible changes in the carbon unoccupied conduction band with $2p$ character, as well as in the carbon plasmon spectral band, for both individual single-wall and individual multiwall carbon nanotubes. Furthermore, for single-walled carbon nanotubes, we see significant changes in the density of states close to the Fermi energy. The observed changes are discussed in the context of increased interatomic spacing, resulting from photon-induced thermal expansion and exciton screening enhancement due to photocarriers. These are the first measurements of photon-induced correlated structural and electronic changes at the atomic level in any nanoscale material. This new capability and technique should enable a new understanding of photon-induced structural, chemical, and electronic reactions across a range of nanoscale systems.

DOI: 10.1103/PhysRevB.87.125403 PACS number(s): 68.37.−d, 61.48.De, 42.60.−v, 79.20.Uv

I. INTRODUCTION

The study of electronic and structural transitions in matter is fundamental to understanding materials properties and performance. While many spectroscopic techniques can provide information on electronic transitions in bulk materials, electron microscopy has inherently higher spatial resolution than optical probe techniques, leading to its extensive use in the study of nanomaterials.[1] In addition to electron-matter interactions studied in the conventional transmission electron microscope (TEM), pioneering experiments performed on pulsed laser ultrafast TEM systems have shed new light on photon-matter interactions at the nanometer scale, including time-resolved measurements of photon-induced structural changes in graphite[2–4] and direct imaging of photon-induced near-field enhancements in plasmonic nanostructures.[5,6] Although the ultrafast and time-resolved experiments provide unique information on high power bursts in short-time intervals and non-linear behavior, not much is known on the steady-state response of materials to an intense continuous beam of light.[7] Motivated by the desire to develop a greater understanding of the structural and electronic behavior of nanoscale materials under intense light, we devised an experimental arrangement to guide an intense, continuous-wave laser beam inside a TEM, ultimately leading to the study of photocatalysis materials. The arrangement is such that the laser is coincident with the electron-beam path near the specimen. The laser addition to the TEM enables the simultaneous characterization and laser pump-probe spectroscopy of nanomaterials at high spatial resolution. We have expanded on previous studies[4] by collecting both high-energy and very low-energy spectral data from laser-illuminated carbon nanotubes (CNTs) in the steady state. We also use three different continuous-wave lasers to excite the structure with infrared (946 nm), green (532 nm), and blue (473 nm) wavelengths. CNTs were selected for analysis because they exhibit interesting photophysical properties, dominated by both electron-electron interactions, in the form of strongly bound excitons,[8] photoluminescence,[9] and electron-phonon interactions.[10] A greater understanding of the unique properties of CNTs, such as their high photoconductivity[11] and photoluminescence[9] can therefore be gained by combining photon-induced excitations with electron microscopy to study the resulting modifications on the CNT lattice and local electronic structure at the nanoscale. In this paper we study photon-induced structural and electronic transitions in individual single-wall (SW) and multi-wall (MW) CNTs in the electron microscope. We measure reversible bond-length changes in individual CNTs, the modification to their unoccupied density of states, and dramatic changes in the excitonic behavior during laser irradiation. This technique promises significant potential in the study of electronic and structural changes in photoexcited nanoscale materials.

II. EXPERIMENTAL DETAILS

In our setup, we combine a continuous-wave diode laser with a TEM (FEI Titan 80-300) equipped with an electron monochromator, a spherical aberration corrector of the imaging lens, and an energy filtering spectrometer. The infrared laser wavelength used here (946 nm) is typical of that used in both resonant Raman spectroscopy and infrared photoconductivity studies. We also carried out measurements using the 532- and 473-nm laser wavelengths, but no significant changes were observed in the CNTs studied. Our TEM is fitted with a specially designed optical port to bring a finely focused laser beam to the sample coincident with a nearly parallel electron beam, allowing coincident and simultaneous exposure of the sample to the electron beam and laser (Fig. 1). The external laser beam is guided to the TEM sample via an optic fiber, collimating tube, focusing lens, and three mirrors to achieve a focused spot at the specimen plane approximately

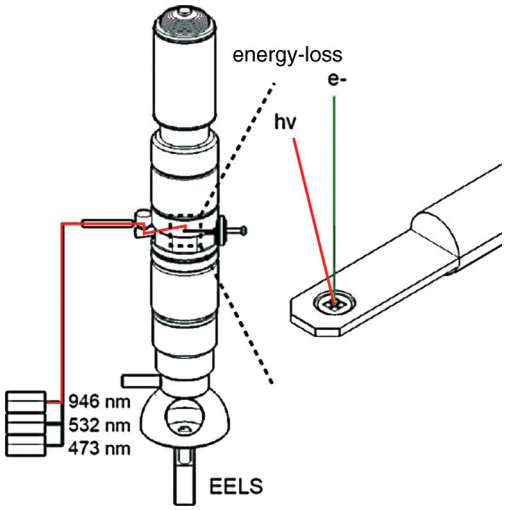

FIG. 1. (Color online) The laser excitation of a CNT in a TEM. Inside the TEM column, the sample is simultaneously probed by both electrons and photons. The electronic structure of the CNT is studied by EELS, where information is contained in the form of energy lost by the fast electron.

5 μm in diameter with an intensity of 4.1×10^6 W/cm^2. SWCNT samples (purchased from NanoIntegris, Cat. No. ISOM-99-P) and MWCNT samples (purchased from Materials & Electrochemical Research (MER) Corporation, Cat. No. MRCMW10) used for this study were prepared for TEM analysis by sonication of the CNT powder in methanol and depositing a few microliters of the dispersion onto a holey carbon TEM grid.

III. RESULTS AND DISCUSSION

A. Electronic transitions under laser illumination

Electron energy-loss spectroscopy (EELS) measurements were performed on a rectangular region enclosing the MWCNT 12.3 nm in diameter, while scanning a monochromated (63-meV energy resolution) electron beam approximately 1 nm in diameter. The MWCNT is composed of 12 walls, each separated by an intergraphitic distance of 0.34 nm, with an inner diameter of 4.4 nm. The selected region was inside a hole in the holey carbon grid, minimizing the influence of the carbon support on measurements. Figure 2 displays the structure and EELS analysis of an individual MWCNT before, during, and after laser illumination. The EELS carbon K-shell signal [Fig. 2(c)] arises from the excitation of carbon 1s electrons to unoccupied anti-bonding-like states above the Fermi energy by the incident fast 80-keV electron. Variations in the energy-loss near-edge structure (ELNES) yield information on how the ionized carbon atom is hybridized, the atom coordination, and its density of states.[12] When interpreting the EEL spectra, it is useful to recall that within the tight-binding model, the electronic structure of MWCNTs is analogous to graphite, which consists of layers of planar sheets, bonded through localized in-plane σ (sp^2) hybridized orbitals and delocalized out-of-plane π (p_z) orbitals, giving rise to a two-band density of electronic states close to the Fermi energy.[13] The ELNES is also strongly modified by excitonic effects, whereby the ejected core electron is influenced by the core hole left behind.[14] The sharp peak at 284 eV in the EEL spectra is due to the transition of a core 1s electron to the π^* anti-bonding orbital, and the

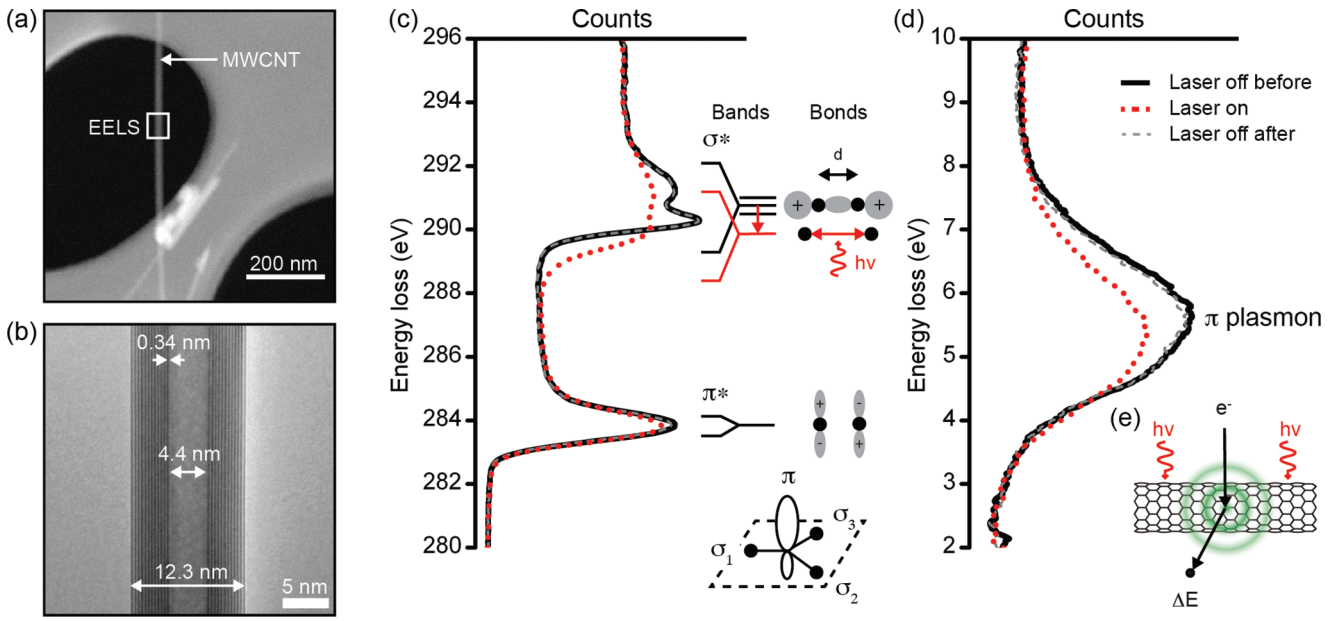

FIG. 2. (Color online) The EELS analysis of a MWCNT before, during, and after laser irradiation in the TEM. (a) The MWCNT, 12.3 nm in diameter, extends over a hole in the carbon support grid. (b) At higher magnification, the structure of the MWCNT from the boxed region is revealed and is free of any obvious defects. The EELS signals in (c) and (d) were obtained from the same boxed region. (c) The changes in the carbon K edge of the MWCNT during laser illumination are perfectly reversible and are strongest in the vicinity of the σ^* peak, which undergoes a redshift. (d) At low-electron energy-loss, the peak belonging to the π^* plasmon undergoes a redshift and reduction in intensity during laser illumination. (e) Schematically, the ejected electron probes the unoccupied states modified by the laser irradiation and modifies the energy-loss of the primary electron that is measured with the spectrometer.

broad peak at 290 eV corresponds to a 1s to σ^* transition. Under laser excitation, we observe a significant modification of the σ^* fine structure from 288–292 eV and a small reduction of the π^* peak. At low electron energy-loss [Fig. 2(d)], the broad peak belonging to the CNT π^* plasmon centered at 5.5 eV is also modified during laser illumination. After laser illumination, the EELS signals are exactly identical to the spectra obtained before laser irradiation. These experiments were carried out on several nanotubes, and the observations are fully reproducible.

B. Nanotube expansion

Shortly after observing the fully reversible changes in the EELS signals, we acquired electron diffraction patterns before, during, and after laser illumination from the same MWCNT (Fig. 3). The diffraction pattern contains detailed information on the MWCNT crystallographic structure. The pattern includes the bright set of {0002} spots along the equatorial line, perpendicular to the nanotube axis, produced by diffraction from the interlayer graphitic planes in the MWCNT, and a hexagonally arranged set of streaked spots from the {10−10} family. The walls of the MWCNT produce Young's slit-like diffraction of the electron beam, with each tube wall behaving like a slit. The multiple slits in the MWCNT introduce an oscillatory envelope to the intensity profile of the

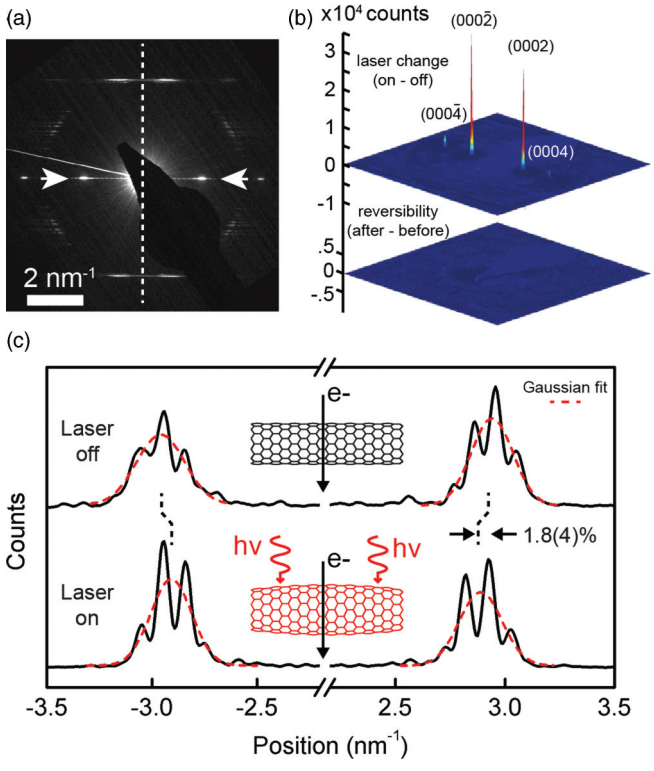

FIG. 3. (Color online) Electron diffraction analysis of a laser-irradiated MWCNT. (a) Detailed structural information is contained in the diffraction pattern. (b) The changes in the CNT diffraction pattern in the {0002} peaks are fully reversible. (c) The intensity profile of {0002} diffraction peaks. During laser illumination, the MWCNT expands radially by 1.8(4)%, shown by displacement of the {0002} diffraction spots. The expansion is exaggerated in the sketch.

{0002} spots [Fig. 3(c)].[15] We observe an inward displacement of the {0002} spots along the equatorial line during irradiation, corresponding to an overall expansion in the radial direction of 1.8(4)%. There is very little difference, however, in the intra-layer diffraction structure to within experimental error because the detection is more sensitive to changes in the overall CNT diameter. The reversible changes in the diffraction pattern during irradiation are highlighted in Fig. 3(c). The redshift of the π plasmon peak is in agreement with the measured expansion, which would result in a slightly reduced average free-electron density.

C. Temperature and core-hole effects

By combining our TEM, EELS, and diffraction measurements, we can provide a framework to understand the structural and electronic changes of the MWCNT during laser illumination. Structurally, the illuminated MWCNT expands in the radial direction by 1.8(4)% measured by electron diffraction. This is likely due to thermal expansion, which corresponds to a temperature rise of 720 K (estimated by using the thermal expansion coefficient $a = 2.5 \times 10^{-5}\,\mathrm{K}^{-1}$),[16] keeping in mind that MWCNTs remain stable at temperatures above 2300 K.[17] Using a dedicated heating sample holder, we attempted to raise the temperature of the sample to 1000 K to repeat the EELS and diffraction measurements on a hot CNT. However, above 570 K, the sample contaminated, preventing interpretable EELS and diffraction analysis at high temperatures. Since the EELS carbon K edge signal reflects, in part, the CNT unoccupied density of states above the Fermi level of p-like symmetry, we measure a redshift in the EELS σ^* antibonding states lying in the C-C plane during illumination. According to the bond orbital approximation model,[18] the electron energy bands in the crystal depend on a set of interatomic matrix elements, which scale with bond length d as d^{-2}. Therefore, an increase in nearest-neighbor spacing d results in a reduction in band energy, shown schematically in Fig. 2(c). The higher-energy σ^* band is more sensitive to bond-length changes due to the strong directionality of the σ carbon-carbon bonds and thus will have a larger redshift than the π^* band upon lattice expansion because of its more delocalized nature. The predictions from this simple model are in agreement with our experimental observations. The second significant electronic modification in the ELNES is the change in shape of the σ^* exciton peak at 290.4 eV during laser irradiation. This effect indicates a significant reduction of the contribution of a core hole on spectral features. Calculations of core-hole effects in the ELNES and x-ray absorption spectra have shown that there is a sharpening of the σ^* peak when the core hole is taken into consideration.[19–21] When a core 1s electron is excited into an unoccupied level by the fast incident electron, a core hole is generated that interacts with the valence and conduction electrons and modifies the crystal electronic structure, if the core hole is not effectively screened.[13] A possible contribution to the change in σ^* could therefore be the significantly more effective screening of the core hole by a larger density of the infrared laser-excited electron-hole carrier pairs,[11] close to the Fermi level. The core-exciton lifetime is also likely reduced at high temperatures, resulting in a weaker exciton peak during the laser irradiation due to

the broadening of such feature. A second thermal effect is the potential contribution of nondipole allowed transitions as observed and calculated in high-temperature x-ray absorption spectroscopy of oxides.[22] Electronic structure calculations of graphite[23] indicate that *s*-like character states in the σ^* region would be present about 0.1 Ry (1.3 eV) below the main *p*-like states of the σ^* peak. These forbidden transitions (due to the EELS selection rules) could potentially give rise to the lower onset of the σ^* peak in the laser-excited spectra. However, our experiments carried out with a reduced laser intensity (achieved with a mechanical chopper at 1 kHz) show that the σ^* energy shift to lower energies is laser-exposure dependent, suggesting that the σ^* peak position during illumination does not arise from a non-dipole transition to the *s*-like states in the C *K* edge. Interestingly, previous *in situ* TEM-EELS studies comparing the EELS signal from bent and straight sections of a MWCNT show similar changes in the C *K* edge structure to what we observe during laser illumination, which are also reversible under loading.[24] The changes are explained through reference to both *ab initio* calculations and to trends in EEL spectra from graphitic structures of increasing curvature and are thus attributed to the increased curvature of graphitic sheets in bent regions.[25] We, however, studied straight nanotubes that remained straight during irradiation, and thus we cannot attribute the same mechanism for our observed changes in the C *K* edge. Our observed CNT expansion would result in a small reduction in curvature, which is in contrast with the trend highlighted previously.[25] A possible explanation is that the changes in electronic structure of a CNT are approximately symmetric under compression/expansion, while localized bending would cause increase in local sp^3 content. The slight reduction of the π^* peak intensity during illumination, small but reproducible, may be due to an increase in carriers in the conduction band. Although the energy resolution can affect the peak intensity, we observe no changes in the width of the peak. We therefore believe that this small effect is not likely an artifact of the measurement. We should also point out that the *p* bands do not represent direct C-C bonds due to the out-of-plane nature of the orbitals, and it is therefore expected to be less sensitive to the bond-length changes. There are no additional features either in proximity of the π^*, such as shoulders or peaks, suggesting that no empty states with the right symmetry are detected from the EELS experiments (i.e., *p*-like character only) in the valence band. At 50% laser illumination strength, the effect on the σ^* is approximately halved with the shift of the inflexion point decreasing in amplitude.

An important consideration is that these underlying physical processes must be present in the steady state. The excitonic effect in the EELS signal is observable if the lifetime of the excited state generated by the laser is of comparable or greater duration than the time between the primary electron interactions with the specimen. Time-resolved fluorescence experiments report a radiative lifetime of over 100 ns for an electron-hole pair in SWCNTs.[26] By comparison, with a measured electron probe current of 0.3 nA, approximately two electrons per nanosecond interact with the specimen in the TEM, giving sufficiently high probability for interaction of the fast electron probing the CNT in the excited state generated by the IR photons from the laser. Given the timescale of primary electrons interacting with the sample and the lifetime of photoinduced high-density carriers that can screen the core hole, we believe that the screening mechanism can play a significant role in the observed changes in the ELNES probed by the electrons sustained under the laser beam, acting as a pump to generate these carriers. No such effects were observed following *in situ* irradiation with high-power green or blue laser beams.

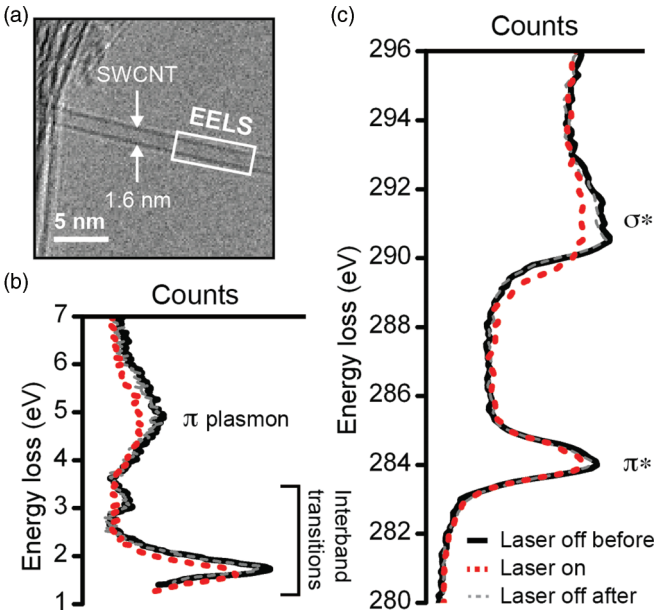

FIG. 4. (Color online) The EELS analysis of a SWCNT before, during, and after laser irradiation in the TEM. (a) The SWCNT, 1.6 nm in diameter, extends over a hole in the support grid. The EELS signals were obtained from the rectangular region highlighted. The reversible changes in low-loss (b) and core-loss (c) EEL spectra of a SWCNT during laser illumination are akin to the changes in the MWCNT spectra.

D. Single-walled CNTs

EELS measurements were also carried out on a SWCNT 1.6 nm in diameter. A rectangular region enclosing a section of the nanotube extending over a hole in the carbon support was thus scanned for EELS analysis (Fig. 4).

In the low-energy-loss spectrum, there is an appreciable and reversible redshift of the spectral features. The strong peak at 1.75 eV shifts to 1.64 eV under laser illumination, and the weaker peak at 3 eV also redshifts and broadens. We assign these peaks to direct interband transitions between the van Hove singularities of the density of states above the Fermi energy, reported previously by scanning tunneling spectroscopy for metallic nanotubes[27] and by *ab initio* calculations of small-diameter single-walled CNTs.[28] These redshifts in the low-electron energy-loss regime are consistent with the predictions of the bond orbital approximation model discussed earlier. Such redshifts have also been observed in air-suspended SWCNTs by photoluminescence spectroscopy with a significantly reduced laser intensity.[29] In that work, the authors proposed that the redshift of the spectral features during laser illumination is due to light-induced molecular deposition onto the nanotube. However, we do not observe

any molecular deposition on the surface of the nanotubes during or after laser illumination from our high-resolution images. Our measurements are also carried out in the high vacuum of the TEM column on nanotube regions that are free from any obvious structural defects or surface adsorbates and are fully reversible. The observed changes are thus unlikely due to molecular deposition on the surface of the nanotube or the formation of structural defects. We also observe a redshift of the collective π plasmon resonance peak from 4.99 to 4.80 eV. As in the case of the MWCNT, we attribute the redshift to the expansion of the tube, causing a small reduction of the average free-electron density of the CNT, thereby reducing the plasma resonance frequency. The EELS core-loss spectrum of the SWCNT bares strong resemblance to the MWCNT spectrum, with π^* and σ^* peaks at 284 and 290 eV, respectively. Despite an increase in signal noise due to the smaller size of the SWCNT, the changes in the EEL spectra during the laser illumination follow the same trend as in the case of the MWCNT: the σ^* band energy is reduced and the π^* intensity is reduced slightly.

IV. CONCLUSIONS

In conclusion, by combining electron microscopy with a laser pump probe, it is possible to explore the change in the nature of chemical bonding transitions in nanoscale materials. When applied to the study of individual CNTs, our results yield information on structural and electronic band structure changes under intense light. We have observed dramatic changes in the *2p* symmetry unoccupied electronic states for both individual MWCNTs and SWCNTs and changes in the excitonic response to the electron-beam-induced excited state due to the change in photocarriers. Changes have also been observed in the density of state singularities near the Fermi energy of SWCNTs. These changes are visible, fully reversible, and are attributed to changes in photocarriers and excitonic lifetimes. This application will be of interest, for example, to understand the unique photoconductivity and luminescence properties of CNTs. More generally, the technique is applicable to the study of excited state transitions in nanomaterials and of interest for studying local electronic changes in nanoscale materials used for photocatalysis applications.

ACKNOWLEDGMENTS

The experimental work presented here was carried out at the Canadian Centre for Electron Microscopy (CCEM), a national facility supported by the Natural Sciences and Engineering Research Council of Canada (NSERC) and McMaster University. We are grateful to G. Radtke for useful discussions on the bond orbital approximation. GAB is grateful to NSERC for a Discovery Grant supporting this work.

*Corresponding author: gbotton@mcmaster.ca

[1] C. Colliex, N. Brun, A. Gloter, D. Imhoff, M. Kociak, K. March, C. Mory, O. Stéphan, M. Tencé, and M. Walls, Philos. Trans. R. Soc. London, Ser. A **367**, 3845 (2009).
[2] O. Kwon, B. Barwick, H. S. Park, J. S. Baskin, and A. H. Zewail, Nano Lett. **8**, 3557 (2008).
[3] F. Carbone, P. Baum, P. Rudolf, and A. H. Zewail, Phys. Rev. Lett. **100**, 035501 (2008).
[4] F. Carbone, O. Kwon, and A. H. Zewail, Science **325**, 181 (2009).
[5] B. Barwick, D. J. Flannigan, and A. H. Zewail, Nature (London) **462**, 902 (2009).
[6] A. Yurtsever, R. M. van der Veen, and A. H. Zewail, Science **335**, 59 (2012).
[7] A. Howie, Eur. Phys. J.: Appl. Phys. **54**, 33502 (2011).
[8] F. Wang, G. Dukovic, L. E. Brus, and T. F. Heinz, Science **308**, 838 (2005).
[9] J. Lefebvre and P. Finnie, Phys. Rev. Lett. **98**, 167406 (2007).
[10] S. Kilina and S. Tretiak, Adv. Funct. Mater. **17**, 3405 (2007).
[11] M. Freitag, Y. Martin, J. A. Misewich, R. Martel, and P. Avouris, Nano Lett. **3**, 1067 (2003).
[12] G. Radke and G. A. Botton, in *Scanning Transmission Electron Microscopy*, edited by S. J. Pennycook and P. D. Nellist (Springer, New York, 2011), p. 207.
[13] J. Bruley, D. B. Williams, J. J. Cuomo, and D. P. Pappas, J. Microsc. **180**, 22 (1995).
[14] P. E. Batson and J. Bruley, Phys. Rev. Lett. **67**, 350 (1991).
[15] M. Kociak, K. Suenaga, K. Hirahara, Y. Saito, T. Nakahira, and S. Iijima, Phys. Rev. Lett. **89**, 155501 (2002).
[16] Y. Maniwa, R. Fujiwara, H. Kira, H. Tou, E. Nishibori, M. Takata, M. Sakata, A. Fujiwara, X. Zhao, S. Iijima, and Y. Ando, Phys. Rev. B **64**, 073105 (2001).
[17] Y. A. Kim, H. Muramatsu, T. Hayashi, M. Endo, M. Terrones, and M. S. Dresselhaus, Chem. Phys. Lett. **398**, 87 (2004).
[18] W. A. Harrison, *Elementary Electronic Structure* (World Scientific, Singapore, 2004).
[19] E. L. Shirley, Phys. Rev. Lett. **80**, 794 (1998).
[20] J. T. Titantah, K. Jorissen, and D. Lamoen, Phys. Rev. B **69**, 125406 (2004).
[21] G. Bertoni and L. Calmels, Micron **37**, 486 (2006).
[22] C. Brouder, D. Cabaret, A. Juhin, and P. Sainctavit, Phys. Rev. B **81**, 115125 (2010).
[23] R. Ahuja, P. A. Brühwiler, J. M. Wills, B. Johansson, N. Mårtensson, and O. Eriksson, Phys. Rev. B **54**, 14396 (1996).
[24] K. Suenaga, C. Colliex, and S. Iilima, Appl. Phys. Lett. **78**, 70 (2001).
[25] K. Suenaga, E. Sandre, C. Colliex, C. J. Pickard, H. Kataura, and S. Iijima, Phys. Rev. B **63**, 165408 (2001).
[26] F. Wang, G. Dukovic, L. E. Brus, and T. F. Heinz, Phys. Rev. Lett. **92**, 177401 (2004).
[27] J. W. G. Wilder, L. C. Venema, A. G. Rinzler, R. E. Smalley, and C. Dekker, Nature (London) **391**, 59 (1998).
[28] A. G. Marinopoulos, L. Reining, A. Rubio, and N. Vast, Phys. Rev. Lett. **91**, 046402 (2003).
[29] P. Finnie and J. Lefebvre, ACS Nano **6**, 1702 (2012).